JOURNAL OF THE
ELECTRON DEVICES SOCIETY

Received 20 December 2019; revised 28 February 2020; accepted 3 April 2020. Date of publication 8 April 2020; date of current version 27 April 2020. The review of this paper was arranged by Editor M. J. Kumar.

Digital Object Identifier 10.1109/JEDS.2020.2986345

Physical Mechanisms of Reverse DIBL and NDR in FeFETs With Steep Subthreshold Swing

CHENGJI JIN (Student Member, IEEE), TAKUYA SARAYA, TOSHIRO HIRAMOTO (Member, IEEE), AND MASAHARU KOBAYASHI (Member, IEEE)

Institute of Industrial Science, University of Tokyo, Tokyo 153-8505, Japan

CORRESPONDING AUTHOR: C. JIN (e-mail: cjjin@nano.iis.u-tokyo.ac.jp)

This work was supported in part by JST PRESTO under Grant 15656058, and in part by MEXT/JSPS Grant-in-Aid under Grant 18H01489.

ABSTRACT We have investigated transient $I_\mathrm{d} - V_\mathrm{g}$ and $I_\mathrm{d} - V_\mathrm{d}$ characteristics of ferroelectric field-effect transistor (FeFET) by simulation with ferroelectric model considering polarization switching dynamics. We show transient negative capacitance (TNC) with polarization reversal and depolarization effect can result in sub-60mV/dec subthreshold swing (SS), reverse drain-induced barrier lowering (R-DIBL), and negative differential resistance (NDR) without traversing the quasi-static negative capacitance (QSNC) region of the S-shaped polarization-voltage ($P - V$) predicted by single-domain Landau theory. Moreover, the mechanisms of R-DIBL and NDR based on the TNC theory are discussed in detail. The results demonstrated in this work can be a possible explanation for the mechanism of previously reported negative capacitance field-effect transistor (NCFET) with sub-60mV/dec SS, R-DIBL, and NDR.

INDEX TERMS Ferroelectric, FET, negative capacitance.

I. INTRODUCTION

Ferroelectric field-effect transistor (FeFET) with sub-60mV/dec subthreshold swing (SS) has become one of the most promising transistor solutions for low-power computing [1]–[3]. Because it has many advantages including (1) high on-state current due to the conventional drift-diffusion carrier transport mechanism, (2) CMOS-compatible material and process thanks to the discovery of ferroelectric HfO_2 [4], [5], and the minimum circuit design modification. Since the physical mechanism of sub-60mV/dec SS is based on negative capacitance (NC) effect of ferroelectric, it is also called negative capacitance field-effect transistor (NCFET). FeFET with sub-60mV/dec SS has been experimentally demonstrated by many research groups [6]–[8]. However, its physical mechanism is still under debate; how NC effect emerges in ferroelectric thin film integrated in the gate stack of FeFET is one of the most important questions which remain to be answered in this research area.

NC effect was originally proposed based on the quasi-static NC (QSNC) theory (Fig. 1 (a)) [1], [2]. For ferroelectric material, there is a meta-stable NC region in the S-shaped polarization-voltage (P-V) predicted by single-domain Landau theory. It was proposed that this NC region can be stabilized by connecting an appropriate paraelectric capacitor [2], [9]. In this way, the S-curve can be traversed bidirectionally without any hysteresis, which makes the idea of developing NCFET possible. However, recently, it was pointed out that sub-60mV/dec SS observed in experiments can be explained by the transient NC (TNC) theory (Fig. 1 (b)) without traversing the QSNC region of the S-curve [10]–[15]. Even with the conventional multi-domain model in which the quasi-static capacitance of ferroelectric is always positive, NC may happen in transient conditions due to the incomplete screening of spontaneous polarization charge [10], [11], [16]–[18]. Note that polarization switching dynamics is responsible for NC effect in transient conditions according to the TNC theory. Therefore, NC effect should be dependent of voltage sweep range and sweep time. It seems that most of sub-60mV/dec SS observed in experiments (at least with hysteresis) can be better explained by the TNC theory in accordance with the dependence of

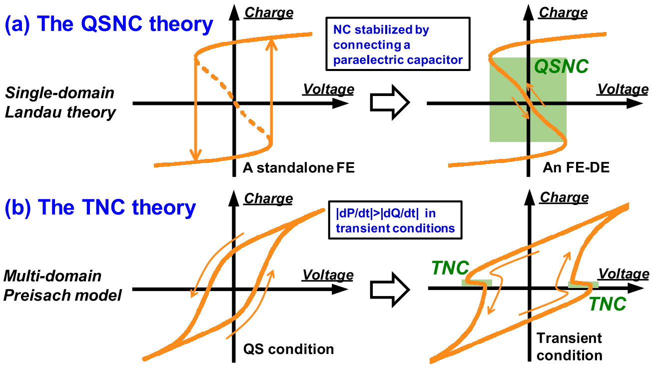

FIGURE 1. **(a) For the QSNC theory, the meta-stable NC region of the S-curve predicted by single-domain Landau theory (the dot line) can be stabilized by connecting an appropriate paraelectric capacitor. In this way, the S-curve can be traversed bidirectionally without any hysteresis, which makes the idea of developing NCFET possible [1], [2]. (b) For the TNC theory, the quasi-static capacitance of ferroelectric is always positive. NC may happen in transient conditions due to the incomplete screening of spontaneous polarization charge [10], [11], [16]–[18].**

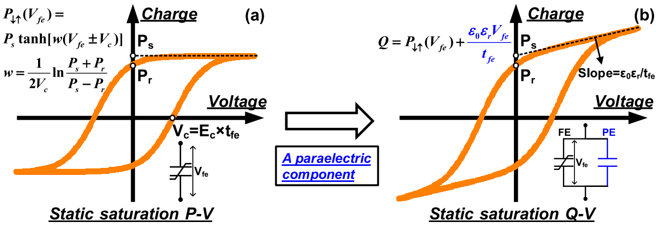

FIGURE 2. **The static saturation (a) $P - V$ and (b) $Q - V$ loops of a ferroelectric capacitor.**

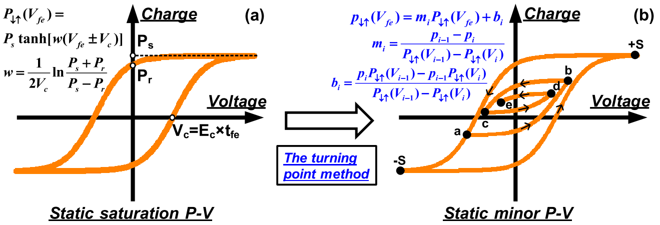

FIGURE 3. **(a) The static saturation $P - V$ loop and (b) the static minor $P - V$ loop of a ferroelectric capacitor.**

the subthreshold characteristics on voltage sweep range and measurement time [8], [11]–[13].

In our previous work, both a ferroelectric-dielectric (FE-DE) series capacitor and FeFET were simulated to investigate the physical mechanism of sub-60mV/dec SS based on the TNC theory [10]. We found that TNC and sub-60mV/dec SS are induced under the condition of $|\mathrm{d}P/\mathrm{d}t| > |\mathrm{d}Q/\mathrm{d}t|$ (depolarization effect) in transient case. In addition, small depletion layer capacitance of FeFET boosts depolarization effect and thus prominent sub-60mV/dec SS in subthreshold region.

FeFET with sub-60mV/dec SS also exhibits unique device characteristics such as reverse drain-induced barrier lowering (R-DIBL) and negative differential resistance (NDR) [6], [19]–[21]. Previously, these special behaviors were predicted by the QSNC theory and regarded as the indication of the stabilized NC in ferroelectric [22]–[24]. The theory of NC needs to give reasonable explanation not only for steep SS but also R-DIBL and NDR consistently. In this work, which is an extended version of [25], we investigate if the TNC theory can also explain R-DIBL and NDR by transient device simulation. In particular, the mechanisms of R-DIBL and NDR based on the TNC theory are discussed in detail according to the simulation results.

This paper is organized as follows. In Section II, the ferroelectric model considering polarization switching dynamics and the simulation methods of transistors are introduced. In addition, a ferroelectric capacitor in response to triangular waveforms is simulated to extract ferroelectric parameters and verify the model. In Section III-A, transient $I_d - V_g$ characteristics of FeFET are simulated and the mechanisms of sub-60mV/dec SS and R-DIBL are discussed in detail based on the TNC theory. Then, in Section III-B, transient $I_d - V_d$ characteristics of FeFET are simulated and the mechanism of NDR is discussed in detail based on the TNC theory. Finally, in Section IV, the conclusion is drawn according to the previous simulation results.

II. MODEL DESCRIPTION AND SIMULATION METHODS

A. FERROELECTRIC MODEL DESCRIPTION

The static saturation polarization-voltage ($P - V$) loop of ferroelectric (Fig. 2 (a)) is described by Miller model which is an analytical version of multi-domain Preisach model [26]. Here, P_s and P_r are saturation and remnant polarization, respectively. V_fe and V_c are voltage across ferroelectric and coercive voltage of ferroelectric, respectively. By considering a paraelectric component, the static saturation charge-voltage ($Q - V$) loop (Fig. 2 (b)) is calculated by the sum of spontaneous polarization and the paraelectric component. Here, ε_r and t_fe are the relative dielectric constant and the thickness of ferroelectric, respectively.

In order to capture minor loops due to partial polarization switching and ferroelectric history, the turning point method is applied [27], [28]. Fig. 3 (b) is an example of minor $P - V$ loops staring from the saturation loop and passing through points a, b, c, d, and e in sequence. The minor loop is calculated according to the last two turning points (($V_{\mathrm{i}-1}$, $p_{\mathrm{i}-1}$) and (V_i, p_i)), as shown by the equations in Fig. 3 (b). Then, the minor $Q - V$ loop can be obtained by considering the paraelectric component, which is the same as the method illustrated in Fig. 2.

Finally, polarization switching delay is introduced to simulate the dynamic behavior of ferroelectric [10], [14]. The delay is determined by a first order differential equation (the equation in Fig. 4) where the switching delay (τ) is a constant. The equivalent circuits of a ferroelectric capacitor in both static and transient conditions are illustrated in Fig. 4. In transient conditions, the actual driving force of spontaneous polarization is the auxiliary voltage (V_aux). There is

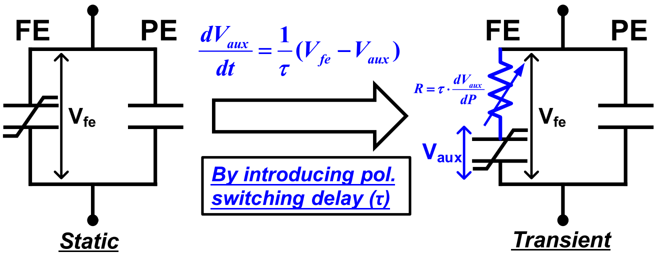

FIGURE 4. Equivalent circuits of a ferroelectric capacitor in both static and transient conditions.

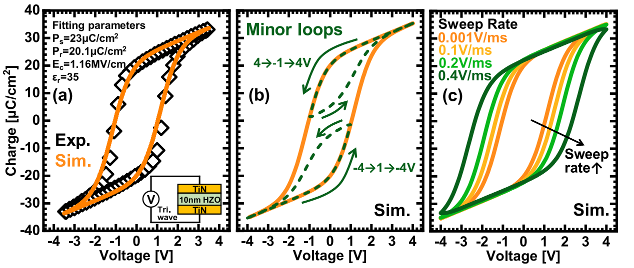

FIGURE 5. (a) The simulated static saturation $Q - V$ with parameters fitting to the measurement result [29]. (b) The simulated static minor $Q - V$ with $+P_s$ and $-P_s$ initialization (4 → −1 → 4 V and −4 → 1 → −4 V). (c) The simulated dynamic $Q - V$ at different sweep rates.

certain delay between V_{aux} and the actual voltage across ferroelectric (V_{fe}).

B. PARAMETER EXTRACTION AND MODEL VERIFICATION

To extract the parameters and verify the abovementioned ferroelectric model, a ferroelectric capacitor in response to triangular waveforms (inset of Fig. 5 (a)) is simulated. Fig. 5 (a) plots the simulated saturation $Q - V$ with parameters fitting to the measurement result [29]. Fig. 5 (b) plots the simulated minor loops with $+P_s$ and $-P_s$ initialization. Fig. 5 (c) plots the dynamic $Q - V$ at different voltage sweep rates. The hysteresis is enlarged at higher sweep rates due to polarization switching delay. Note that the value of τ is assumed to be 4 msec in this work, since the recent measurement shows τ of ferroelectric HfO_2 can be in msec scale [15]. Assuming other value of τ does not qualitatively affect the conclusion of this work.

C. SIMULATION METHODS OF TRANSISTORS

Fig. 6 (a) illustrates the simulated device structures and parameters. Both FeFET and reference MOSFET are simulated. The only difference between them is the additional $HfZrO_2$ (HZO) thin film in the gate stack of FeFET.

Fig. 6 (b) shows the flow chart for transistor simulation. Before transient $I_d - V_g$ and $I_d - V_d$ simulation, quasi-static (QS) sweep is applied to initialize certain polarization states and bias conditions. After that, double V_g or V_d sweep is applied in transient conditions. Note that the value of V_{max} in Fig. 6 (b) is large enough to initialize saturation polarization (P_s) in this study.

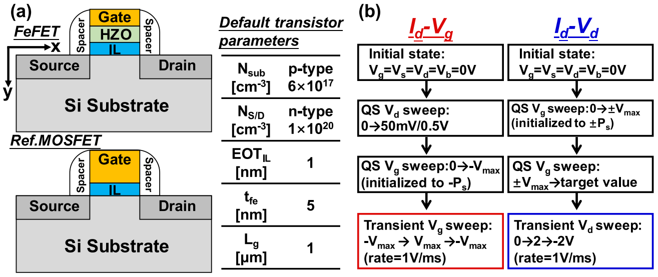

FIGURE 6. (a) The simulated device structures and parameters. (b) The flow chart for both $I_d - V_g$ and $I_d - V_d$ simulation.

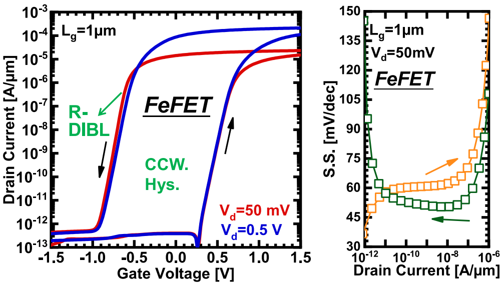

FIGURE 7. The simulated transient $I_d - V_g$ characteristics and the calculated $SS - I_d$ for FeFET.

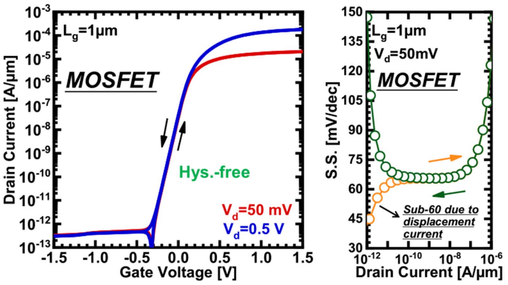

FIGURE 8. The simulated transient $I_d - V_g$ characteristics and the calculated $SS - I_d$ for reference MOSFET.

III. RESULT AND DISCUSSION

A. $I_D - V_G$ CHARACTERISTICS AND R-DIBL

Fig. 7 and 8 plot the simulated transient $I_d - V_g$ characteristics and the calculated $SS - I_d$ for FeFET and reference MOSFET, respectively. FeFET shows counterclockwise hysteresis in I_d, which is caused by polarization switching. Meanwhile, prominent sub-60mV/dec SS and R-DIBL are observed in reverse sweep. Whereas reference MOSFET shows hysteresis-free operation. Note that sub-60mV/dec SS appears to occur at low I_d in forward sweep even for MOSFET. This is due to the fact that I_d at the drain electrode consists of both drift-diffusion current and displacement current which is charging/discharging current of the gate-to-drain capacitor in transient condition. During forward V_g sweep, the directions of these two current components are opposite, thus making SS lower than 60mV/dec.

To confirm the physical origin of sub-60mV/dec SS, Fig. 9 (a) plots the polarization switching current ($|dP/dt|$), the total free charge current ($|I_g| = |dQ/dt|$) flowing through

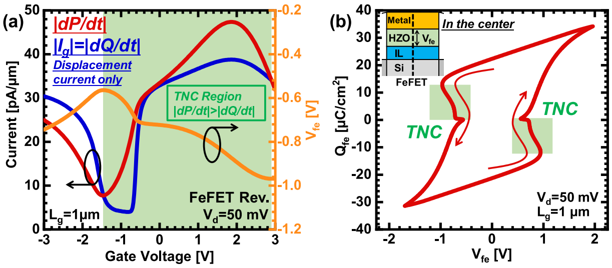

FIGURE 9. (a) The polarization switching current ($|dP/dt|$), the total free charge current ($|I_g| = |dQ/dt|$) flowing through the gate, and voltage across ferroelectric (V_{fe}) during reverse V_g sweep. (b) The extracted $Q_{fe} - V_{fe}$ during double V_g sweep shows TNC as well.

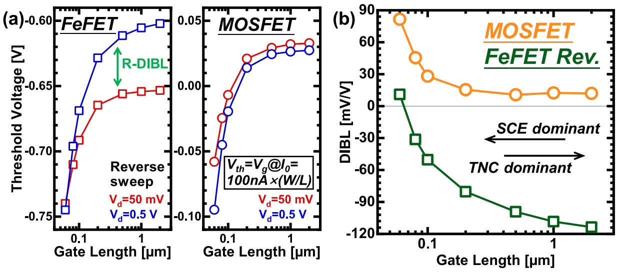

FIGURE 10. (a) The threshold voltage (V_{th}) at $V_d = 50$ mV and 0.5 V as a function of gate length (L_g). (b) DIBL as a function of L_g.

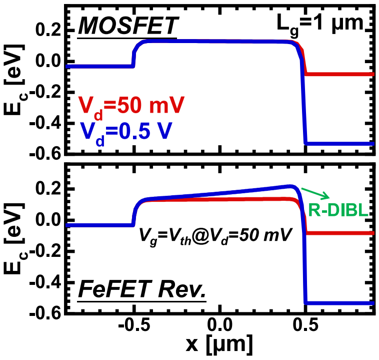

FIGURE 11. Extracted conduction band-edge energies (E_c). R-DIBL can be judged by the increased barrier height at higher V_d.

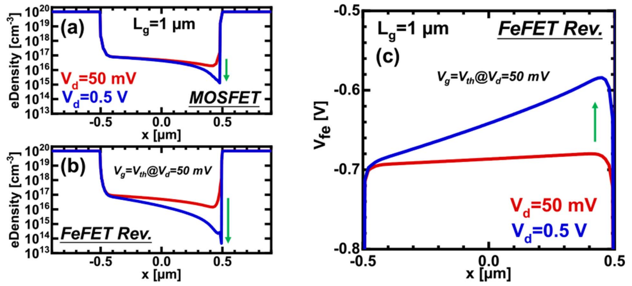

FIGURE 12. Simulated charge density in the channel (N_{ch}) at different V_d for (a) reference MOSFET and (b) FeFET. (c) Voltage across ferroelectric (V_{fe}) at different V_d.

the gate, and voltage across ferroelectric (V_{fe}) during reverse V_g sweep. Note that here I_g is only induced by displacement current and there is no other leakage component, because the insulator is assumed to be ideal in this simulation. In certain V_g region, $|dP/dt|$ is larger than $|I_g| = |dQ/dt|$ (green shade in Fig. 9 (a)), leading to TNC and SS improvement [10], [17], [30]. This can be better understood by considering the charge balance condition: $Q = \varepsilon_0 \varepsilon_r V_{fe}/t_{fe} + P$. Once $|dP/dt|$ is larger than $|I_g| = |dQ/dt|$, the signs of dV_{fe}/dt and dV_g/dt are opposite and TNC occurs. In other words, the depolarization effect caused by the switched spontaneous polarization results in TNC, if the screening by free charge at the gate electrode cannot response fast enough. Moreover, both $|dP/dt|$ and $|I_g| = |dQ/dt|$ are suppressed by small depletion capacitance in subthreshold region [10], which is consistent with the experimental result in [31]. The extracted $Q_{fe} - V_{fe}$ also exhibits TNC in certain region, as shown in Fig. 9 (b). Since the TNC region (green shade in Fig. 9 (b)) covers more of the subthreshold region (the low positive charge region in Fig. 9 (b)) in the transition from inversion region to depletion region during the reverse sweep than in the transition from accumulation region to depletion region during the forward sweep, sub-60mV/dec SS is prominently observed in reverse sweep in experiments [7], [8], [21].

Fig. 10 (a) and (b) plot the threshold voltage (V_{th}) and DIBL as a function of gate length (L_g) for both FeFET and reference MOSFET. For FeFET with long L_g, as V_d increases V_{th} becomes higher and the value of DIBL is negative. This phenomenon is opposite to conventional MOSFET and regarded as R-DIBL. As L_g decreases, DIBL of FeFET gradually increases and becomes close to zero due to the short channel effect (SCE) and finally becomes positive due to the dominant SCE. R-DIBL can be also judged by the increased barrier height as shown in Fig. 11.

To explore the mechanism of R-DIBL, we investigated the charge density in the channel (N_{ch}) and the voltage across the ferroelectric layer (V_{fe}) at different V_d (Fig. 12). For fixed V_g, higher V_d will lead to higher channel potential and thus lower N_{ch} and more depletion near the drain. This happens even for conventional MOSFET (Fig. 12 (a)). However, for FeFET, higher V_d (lower N_{ch} and more depletion) will result in higher V_{fe} (reduced $|V_{fe}|$) due to TNC (Fig. 12 (b)). The increased V_{fe} will further decrease N_{ch} (Fig. 12 (c)), raise the channel electron potential shown in Fig. 11, and thus I_d decreases. In this way, R-DIBL happens.

B. I_D-V_D CHARACTERISTICS AND NDR

Fig. 13 (a) and (b) plot the simulated transient $I_d - V_d$ characteristics for FeFET with $+P_s$ (low V_{th}) and $-P_s$ (high V_{th}) initialization, respectively. In the case of $+P_s$ initialization, I_d shows large hysteresis. Moreover, I_d decreases as V_d increases in forward V_d sweep, which is regarded as NDR. However, in the case of $-P_s$ initialization, I_d is nearly hysteresis-free and no NDR is observed. These results are consistent with experiments demonstrated in [21].

Fig. 14 (a) plots $I_d - V_d$ in forward sweep at $V_g = 0.3$ V with different L_g when $+P_s$ is initialized. To observe the L_g

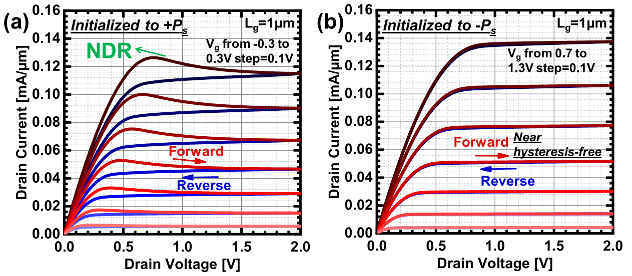

FIGURE 13. The simulated transient $I_d - V_d$ characteristics for FeFET with (a) $+P_s$ (low V_{th}) and (b) $-P_s$ (high V_{th}) initialization. NDR is observed only in forward V_d sweep with $+P_s$ initialization.

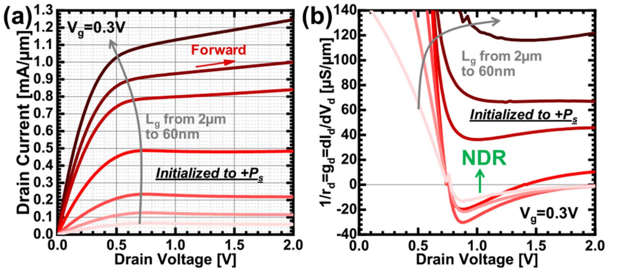

FIGURE 14. (a) The simulated $I_d - V_d$ in forward sweep at $V_g = 0.3$ V with different L_g when $+P_s$ is initialized. (b) The corresponding reciprocal of differential resistances ($1/r_d = g_d = dI_d/dV_d$).

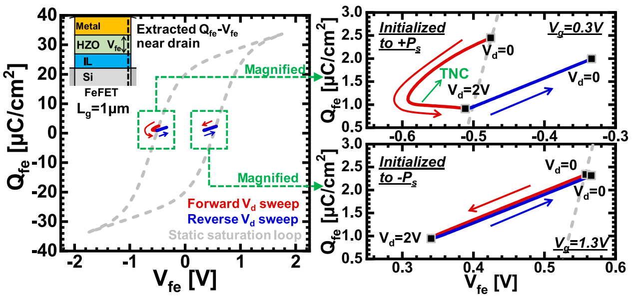

FIGURE 15. Extracted $Q - V$ trajectory of ferroelectric ($Q_{fe} - V_{fe}$) during the transient V_d sweep. The magnified plots are shown in the right side.

dependence of NDR more clearly, the corresponding reciprocal of differential output resistances ($1/r_d = g_d = dI_d/dV_d$) are calculated (Fig. 14 (b)). As L_g scales down, NDR is first strong, then becomes weaker, and finally disappears, which is due to the competition between TNC and SCE.

According to the simulated $I_d - V_d$ characteristics (Fig. 13), ferroelectric history should play an important role in NDR. Therefore, we investigated the $Q - V$ trajectory of ferroelectric ($Q_{fe} - V_{fe}$) near the drain during the transient V_d sweep (Fig. 15). Note that TNC can be induced during V_d sweep instead of V_g sweep. In the case of $+P_s$ initialization, $Q_{fe} - V_{fe}$ during V_d sweep shows large hysteresis and TNC is observed only in forward V_d sweep because there is a pathway where Q_{fe} decreases while V_{fe} increases as a part of saturation loop. Whereas, in the case of $+P_s$ initialization, $Q_{fe} - V_{fe}$ during V_d sweep is nearly hysteresis-free and no TNC is observed because there is no pathway where Q_{fe} increases while V_{fe} decreases in a minor loop. The behaviors of $Q_{fe} - V_{fe}$ are consistent with $I_d - V_d$ (Fig. 13), which means TNC is responsible for NDR observed in forward sweep, if $+P_s$ is initialized.

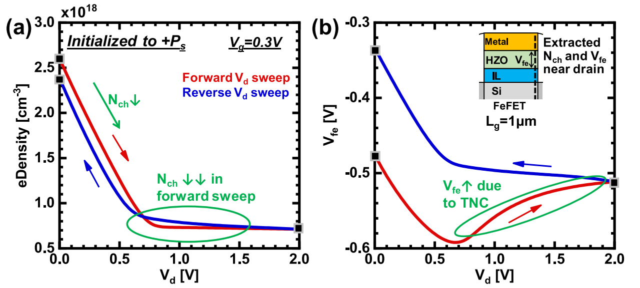

FIGURE 16. (a) N_{ch} and (b) V_{fe} near the drain during the transient V_d sweep.

The mechanism of NDR is similar to R-DIBL shown in the previous part and it can be illustrated as follows. Fig. 16 (a) and (b) plot N_{ch} and V_{fe} near the drain during the transient V_d sweep, respectively. For fixed V_g, as V_d increases, N_{ch} decreases and the channel near the drain depletes more due to the increased channel potential near the drain (Fig. 16 (a)). Then, in TNC region, V_{fe} increases (Fig. 16 (b)) according to the charge balance condition. This increased V_{fe} further reduces N_{ch} near the drain (Fig. 15 (a)), electron potential is raised, and I_d decreases. Therefore, NDR happens. This can be also interpreted as R-DIBL in that V_{th} increases and thus I_d decreases as V_d increases.

IV. CONCLUSION

According to the TNC theory, NC effect and sub-60mV/dec SS of FeFET are induced by the incomplete screening of spontaneous polarization charge ($|dP/dt| > |dQ/dt|$) in transient condition, which is different from the QSNC theory where stabilized S-curve is traversed bidirectionally without hysteresis. In this work, transient $I_d - V_g$ and $I_d - V_d$ characteristics of FeFET are simulated based on the TNC theory and the calibrated parameters of ferroelectric HfO_2. Simulation results were able to reproduce not only sub-60mV/dec SS but also R-DIBL and NDR. By investigating N_{ch} and V_{fe} near the drain, we find that TNC boots the decreasing of N_{ch} and raising the channel electron potential near the drain as V_d increases, leading to R-DIBL and NDR. The TNC theory illustrated in this work can be a possible explanation for the mechanisms of previously reported NCFET with sub-60mV/dec SS, R-DIBL, and NDR.

REFERENCES

[1] S. Salahuddin and S. Datta, "Use of negative capacitance to provide voltage amplification for low power nanoscale devices," *Nano Lett.*, vol. 8, no. 2, pp. 405–410, 2008, doi: 10.1021/nl071804g.

[2] A. I. Khan, C. W. Yeung, C. Hu, and S. Salahuddin, "Ferroelectric negative capacitance MOSFET: Capacitance tuning & antiferroelectric operation," in *IEDM Tech. Dig.*, Washington, DC, USA, Dec. 2011, pp. 3–11, doi: 10.1109/IEDM.2011.6131532.

[3] M. Kobayashi, "A perspective on steep-subthreshold-slope negative-capacitance field-effect transistor," *Appl. Phys. Exp.*, vol. 11, no. 11, pp. 1–20, Oct. 2018, doi: 10.7567/APEX.11.110101.

[4] T. S. Böscke, J. Müller, D. Bräuhaus, U. Schröder, and U. Böttger, "Ferroelectricity in hafnium oxide thin films," *Appl. Phys. Lett.*, vol. 99, no. 10, Art. no. 102903, 2017, doi: 10.1063/1.3634052.

[5] J. Müller *et al.*, "Ferroelectricity in simple binary ZrO_2 and HfO_2," *Nano Lett.*, vol. 12, no. 8, pp. 4318–4323, 2012, doi: 10.1021/nl302049k.

[6] M. H. Lee *et al.*, "Extremely steep switch of negative-capacitance nanosheet GAA-FETs and FinFETs," in *IEDM Tech. Dig.*, San Francisco, CA, USA, Dec. 2018, pp. 1–4, doi: 10.1109/IEDM.2018.8614510.

[7] M. N. K. Alam *et al.*, "On the characterization and separation of trapping and ferroelectric behavior in HfZrO FET," *IEEE J. Electron Devices Soc.*, vol. 7, pp. 855–862, Mar. 2019, doi: 10.1109/JEDS.2019.2902953.

[8] P. Sharma *et al.*, "Impact of total and partial dipole switching on the switching slope of gate-last negative capacitance FETs with ferroelectric hafnium zirconium oxide gate stack," in *Proc. IEEE Symp. VLSI Technol.*, Kyoto, Japan, Jun. 2017, pp. T154–T155, doi: 10.23919/VLSIT.2017.7998160.

[9] H. Agarwal *et al.*, "Proposal for capacitance matching in negative capacitance field-effect transistors," *IEEE Electron Device Lett.*, vol. 40, no. 3, pp. 463–466, Mar. 2019, doi: 10.1109/LED.2019.2891540.

[10] C. Jin, T. Saraya, T. Hiramoto, and M. Kobayashi, "On the physical mechanism of transient negative capacitance effect in deep subthreshold region," *IEEE J. Electron Devices Soc.*, vol. 7, pp. 368–374, Feb. 2019, doi: 10.1109/JEDS.2019.2899727.

[11] P. Sharma, J. Zhang, K. Ni, and S. Datta, "Time-resolved measurement of negative capacitance," *IEEE Electron Device Lett.*, vol. 39, no. 2, pp. 272–275, Feb. 2018, doi: 10.1109/LED.2017.2782261.

[12] B. Obradovic, T. Rakshit, R. Hatcher, J. A. Kittl, and M. S. Rodder, "Ferroelectric switching delay as cause of negative capacitance and the implications to NCFETs," in *Proc. Symp. IEEE VLSI Technol.*, Honolulu, HI, USA, Jun. 2018, pp. T51–T52.

[13] B. Obradovic, T. Rakshit, R. Hatcher, J. A. Kittl and M. S. Rodder, "Modeling transient negative capacitance in steep-slope FeFETs," *IEEE Trans. Electron Devices*, vol. 65, no. 11, pp. 5157–5164, Nov. 2018, doi: 10.1109/TED.2018.2868479.

[14] A. K. Saha, S. Datta, and S. K. Gupta, "Negative capacitance' in resistor-ferroelectric and ferroelectric-dielectric networks: Apparent or intrinsic?" *J. Appl. Phys.*, vol. 123, no. 10, 2018, Art. no. 105102, doi: 10.1063/1.5016152.

[15] H. Wang *et al.*, "New insights into the physical origin of negative capacitance and hysteresis in NCFETs," in *IEDM Tech. Dig.*, San Francisco, CA, USA, Dec. 2018, pp. 1–4, doi: 10.1109/IEDM.2018.8614504.

[16] P. Zubko *et al.*, "Negative capacitance in multidomain ferroelectric superlattices," *Nature*, vol. 534, no. 7608, pp. 524–528, Jun. 2016, doi: 10.1038/nature17659.

[17] S.-C. Chang, U. E. Avci, D. E. Nikonov, S. Manipatruni, and I. A. Young, "Physical origin of transient negative capacitance in a ferroelectric capacitor," *Phys. Rev. Appl.*, vol. 9, Jan. 2018, Art. no. 014010, doi: 10.1103/PhysRevApplied.9.014010.

[18] Q. Han *et al.*, "Subthreshold behavior of floating-gate MOSFETs with ferroelectric capacitors," *IEEE Trans. Electron Devices*, vol. 65, no. 10, pp. 4641–4645, Oct. 2018, doi: 10.1109/TED.2018.2863727.

[19] H. Zhou *et al.*, "Negative capacitance, n-channel, Si FinFETs: Bi-directional sub-60 mV/dec, negative DIBL, negative differential resistance and improved short channel effect," in *Proc. IEEE Symp. VLSI Technol.*, Honolulu, HI, USA, Jun. 2018, pp. 53–54, doi: 10.1109/VLSIT.2018.8510691.

[20] J. Zhou *et al.*, "Frequency dependence of performance in Ge negative capacitance PFETs achieving sub-30 mV/decade swing and 110 mV hysteresis at MHz," in *IEDM Tech. Dig.*, San Francisco, CA, USA, Dec. 2017, pp. 1–4, doi: 10.1109/IEDM.2017.8268397.

[21] M. Jerry, J. A. Smith, K. Ni, A. Saha, S. Gupta, and S. Datta, "Insinhts on the DC characterization of ferroelectric field-effect-transistors," in *Proc. 76th Device Res. Conf. (DRC)*, Santa Barbara, CA, USA, 2018, pp. 1–2, doi: 10.1109/DRC.2018.8442191.

[22] H. Ota, T. Ikegami, J. Hattori, K. Fukuda, S. Migita, and A. Toriumi, "Fully coupled 3-D device simulation of negative capacitance FinFETs for sub 10 nm integration," in *IEDM Tech. Dig.*, San Francisco, CA, USA, Dec. 2016, pp. 1–4, doi: 10.1109/IEDM.2016.7838403.

[23] A. K. Saha, P. Sharma, I. Dabo, S. Datta, and S. K. Gupta, "Ferroelectric transistor model based on self-consistent solution of 2D poisson's, non-equilibrium green's function and multi-domain Landau Khalatnikov equations," in *IEDM Tech. Dig.*, Dec. 2017, pp. 1–4, doi: 10.1109/IEDM.2017.8268385.

[24] G. Pahwa, A. Agarwal, and Y. S. Chauhan, "Numerical investigation of short-channel effects in negative capacitance MFIS and MFMIS transistors: Subthreshold behavior," *IEEE Trans. Electron Devices*, vol. 65, no. 11, pp. 5130–5136, Nov. 2018, doi: 10.1109/TED.2018.2870519.

[25] C. Jin, T. Saraya, T. Hiramoto, and M. Kobayashi, "Transient negative capacitance as cause of reverse drain-induced barrier lowering and negative differential resistance in ferroelectric FETs," in *Proc. IEEE Symp. VLSI Technol.*, Kyoto, Japan, Jun. 2018, pp. T220–T221, doi: 10.23919/VLSIT.2019.8776583.

[26] S. L. Miller, J. R. Schwank, R. D. Nasby, and M. S. Rodger, "Modeling ferroelectric capacitor switching with asymmetric nonperiodic input signals and arbitrary initial conditions," *J. Appl. Phys.*, vol. 70, no. 5, pp. 2849–2860, 1991, doi: 10.1063/1.349348.

[27] B. Jiang, P. Zurcher, R. E. Jones, S. J. Gillespie, and J. C. Lee, "Computationally efficient ferroelectric capacitor model for circuit simulation," in *Proc. IEEE Symp. VLSI Technol.*, Kyoto, Japan, Jun. 1997, pp. 141–142, doi: 10.1109/VLSIT.1997.623738.

[28] K. Ni, M. Jerry, J. A. Smith, and S. Datta, "A circuit compatible accurate compact model for ferroelectric-FETs," in *Proc. IEEE Symp. VLSI Technol.*, Honolulu, HI, USA, Jun. 2018, pp. T131–T132.

[29] M. Kobayashi, N. Ueyama, K. Jang, and T. Hiramoto, "Experimental study on polarization-limited operation speed of negative capacitance FET with ferroelectric HfO_2," in *IEDM Tech. Dig.*, San Francisco, CA, USA, Dec. 2016, pp. 1–4, doi: 10.1109/IEDM.2016.7838402.

[30] J. Gomez, S. Dutta, K. Ni, S. Joshi, and S. Datta, "Steep slope ferroelectric field effect transistor," in *Proc. Electron Devices Technol. Manuf. Conf. (EDTM)*, Singapore, 2019, pp. 59–61, doi: 10.1109/EDTM.2019.8731115.

[31] C. Jin, K. Jang, T. Saraya, T. Hiramoto, and M. Kobayashi, "Experimental study on the role of polarization switching in subthreshold characteristics of HfO_2-based ferroelectric and anti-ferroelectric FET," in *IEDM Tech. Dig.*, San Francisco, CA, USA, Dec. 2018, pp. 1–4, doi: 10.1109/IEDM.2018.8614486.